

# Digital optical phase conjugation generalized in integrated optics

Claver Havyarimana

<sup>1</sup> Physics department, Faculty of Sciences, University of Burundi, Bujumbura, BP 2700 Burundi.

<sup>2</sup> Research Center in Mathematics and Physics (RCMP).

\* Auteur de correspondance: Email / [claver.havyarimana@ub.edu.bi](mailto:claver.havyarimana@ub.edu.bi)

Received on: October 11<sup>th</sup> 2021

Accepted for publication on: March 25<sup>th</sup> 2022

Published online for the first time on: March 31<sup>st</sup> 2022

## Abstract

Planar waveguide-based digital optical phase conjugation (DOPC) is investigated and generalized in backward and forward direction. Theoretical investigation based on reciprocity of an optical path principle is followed by finite difference time domain (FDTD) numerical simulations. By an appropriate design, multimode interferometer and reflected Bragg grating are used here, it is shown that DOPC allows to reconstruct the light field at the place where the light is inputted for backward direction and at the corresponding port in forward direction. Devices designed on DOPC would be of high performance as the one dimensional distribution shows.

**Keywords:** *Planar waveguide, integrated optics, digital optical phase conjugation.*

---

## Résumé

La conjugaison de phase optique numérique (DOPC) basée sur un guide d'ondes plan est étudiée et généralisée dans la direction en arrière et vers l'avant. L'investigation théorique basée sur la réciprocity d'un principe de chemin optique est suivie de simulations numériques dans le domaine temporel des différences finies (FDTD). Par une conception appropriée, l'interféromètre multimode et le réseau de Bragg réfléchi sont utilisés ici, il est montré que le DOPC permet de reconstruire le champ de lumière à l'endroit où la lumière est entrée pour la direction arrière et au port correspondant dans la direction vers l'avant. Les dispositifs conçus sur DOPC seraient de haute performance comme le montre la distribution en une dimension.

**Keywords:** *Guide d'onde plan, optique intégrée, conjugaison de phase optique numérique.*

---

## 1. Introduction

When the phase of an optical wavefront is forced to change to its conjugation, the wave would go back as if time was inverted. This phenomenon was first observed in 1970s and named as optical phase conjugation (OPC) (Yariv A & Yeh P, 1978). The reflected light by a regular mirror depends on the incident angle while the light reflected by a phase conjugate mirror goes straight back the way it came independently of the incident angle. OPC can be implemented by many processes like four wave mixing, backward stimulated Brillouin, Raman, Rayleigh-wing or Kerr scattering process.<sup>2</sup> The most used method is degenerated four-wave mixing (FWM) (Guang S. He, 2002; Feinberg J and Hellwarth R. W, 1980; Lindsay, 1987 and Yeh P, 1993).

The propagation control of the optical wave allowed by OPC made the method of great interest. However, the use of photorefractive material is its main drawback. A method with no such requirement is more efficient. Digital optical phase conjugation (DOPC) is just the method. In addition to non-use of nonlinear material, DOPC allows digital control of the light propagation. DOPC has then number of advantages over conventional OPC: 1) as an adaptive optics method, the power of the generated OPC wave is independent of the input signal and can be freely adjusted; 2) the same DOPC system can in principle work with both continuous wave (CW) and pulsed laser systems at any power levels; 3) Fast and more flexible and 4) Doesn't need nonlinear medium.

In 2010, Meng Cui et al. reported a new technique for wave front reconstruction which doesn't require nonlinear medium (Meng C and Changhui Y, 2010). The technique has an optoelectronic nature and is called DOPC. Their system consists of two parties: a Charge Coupled Device (CCD) or Complementary Metal-oxide Semiconductor (CMOS) camera for wavefront recording and a spatial-light modulator (SLM) for wavefront playback. SLM consist of an array of pixels, each of which can individually control the phase or amplitude of light passing through it or reflecting off it. These two components are precisely aligned around a beam splitter to optically situate the two digital components in the same optical position. The DOPC procedure follows two steps: (1) the wavefront of the input beam is measured on a scientific CMOS (sCMOS) sensor array using either phase-

shifting holography or off-axis holography; and (2) the conjugated copy of the measured wavefront is displayed on an SLM. Since the pixel size of a SLM is much larger than optical wavelength, the systems can reconstruct only slowly varying optical wavefronts.

In the same year, Zhiyang Li reported how to use a taper made up with a bundle of optical fibers to decompose an incident wavefront before it is reconstructed by SLM (Zhiyang Li, 2010). Since the decomposed incident light are led to isolated single mode fibers at wide end of the taper as fundamental modes, the conjugate optical fields of these fundamental modes can be reconstructed accurately by SLMs. Due to reciprocity of an optical path, these conjugate fundamental modes go back and combine to regenerate the incident light field. The author proved theoretically that for any incident optical wavefronts, whether it is varying very slowly or rapidly, the reconstructed field can attain a diffraction limited resolution, much higher than when only bare SLM is used. Two reflective (liquide crystal on sillicium) LCOS SLMs, SLM1 and SLM2, working in phase-mostly mode were placed behind a beam splitter. Their pixels were aligned accurately with each other and coupled to the cores of single-mode fibers of the taper by optical lens L2 and micro-lens-array MLA. Via vector addition, SLM1 together with SLM2 can reconstruct the desired conjugate fundamental modes within the core of each single mode fiber. Reference 7 contains more details for the interested.

Both works mentioned above and others like (Zhiyang L, 2013; Songcan L and Mark N A, 2000.; Hsieh C.L, et al,2010. ; Yuecheng S, Yan L, Cheng M ; Lihong V. W, 2016; Daifa W & al, 2015 ; Yu,Z et al, 2019 ; Kai Z et al, 2020 ; Zhongtao Cheng et al ,2020 ; Chaojie Ma et 2018 ; Ivo M. Vellekoop et al 2012 ; Hillman, T et al 2013 and Daifa Wang et al 2015) employed SLMs to generate conjugate optical fields for 3D wavefront reconstruction in free space. In this paper, we will demonstrate how to implement DOPC in Integrated optics for planar optical circuits for backward and forward directions. In our previous works (Zhiyang L and Havyarimana C, 2013; Havyarimana C and Zhiyang L, 2015), we have demonstrated DOPC implementation in integrated optics even its application in optical switching but only in backward direction. Here the work show the generalization in both backward and forward direction.

Integrated optics is the base of the technology of packaging multiple optical devices on a single platform (Miller S.E, 1969). Planar waveguide is the basic component in integrated optics. Its structure has a high-

refractive index core surrounded by lower cladding to guide light beams. The technology began with the proposition of Steward Miller in 1969 to fabricate photonic integrated circuits similarly to microelectronic ones.<sup>8</sup> Since then, researchers in optical communication community have worked on generation, transportation, amplification, modulation, switching and detection of light signal in integrated fashion. The major advantage of optical integration compared to non-integrated components are reduced packaging cost, reduced fiber coupling loss, reduced power consumption, small size, stability and reproducibility.

Devices on planar lightwave circuits (PLCs) are generally arranged in planar manner and are connected to each other via optical waveguides. Some of these devices are: optical switches where a large number of individual switch elements are integrated onto the same substrate; Laser arrays known as “Multiwavelength Lasers” and Wavelength division multiplexing receiver assemblies consisting of Arrayed waveguide gratings (AWG) with an amplifier and multiple PIN (positive intrinsic negative) diode receivers in the same assembly.

The following sections concern DOPC implementation in integrated optics beginning with theoretical investigation followed by numerical simulations.

## 2. Planar waveguide-based backward digital optical phase conjugation

### 2.1. Design of waveguide structure for DOPC

A light field in a complex waveguide device consists of many eigenmodes. There is no way to modulate all these eigenmodes simultaneously for implementation of DOPC. To perform DOPC, we need: 1) a waveguide structure to decompose all the eigenmodes into a number of single mode waveguides so that they can be handled individually; 2) an element in each single mode waveguide to reverse, or reflect the fundamental eigenmode and 3) an element in each single mode waveguide to modulate the phase of the reflected fundamental eigenmode to its conjugation.

Figure 1 illustrated a generalized design fulfilling above requirements for DOPC implementation. As illustrated in Fig.1, the device has M isolated single-mode waveguides at left side and N isolated single-mode waveguides at right side. Between them, there is an adiabatic waveguide structure (AWS) for decomposition. On each single-mode waveguide at the right side there are elements marked as PS (phase shift)

for phase modulation and distributed Bragg grating (DBG) to reflect back the mode of wavelength  $\lambda$ .

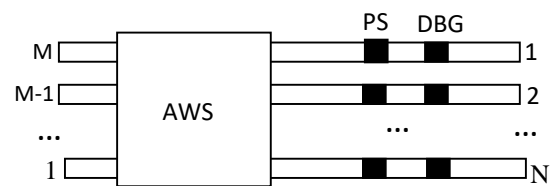


**Figure 1.** General Structure for waveguide-based DOPC implementation

### 2.2. Reciprocity of an optical path

In this section we examine how optical conjugate waves travel in waveguide devices to see whether DOPC could be implemented and under what condition. In Fig.1, the light fields propagating rightwards  $\lambda$  at both left and right sides of AWS could be expressed by column vectors  $\Psi_{left}=[a_1, a_2, \dots, a_M]^T$  and  $\Psi_{right}=[b_1, b_2, \dots, b_N]^T$ , where  $a_i$  and  $b_j$  are complex amplitudes of fundamental eigenmodes within each isolated single-mode waveguide at left side and right side respectively. If AWS is adiabatic, reflected backward field is negligible. Then following Eq.1 the field at right side  $\Psi_{right}$  could be related to field at left side  $\Psi_{left}$  by,

$$\Psi_{right} = \mathbf{T} \Psi_{left} \quad (1)$$

where  $\mathbf{T}$  is a  $N \times M$  transmission matrix of the AWS for light field propagating from left side to right side,

$$\mathbf{T} = \begin{pmatrix} \varphi_{1,1} & \varphi_{1,2} & \dots & \varphi_{1,M} \\ \varphi_{2,1} & \varphi_{2,2} & \dots & \varphi_{2,M} \\ \dots & \dots & \varphi_{i,j} & \dots \\ \varphi_{N,1} & \varphi_{N,2} & \dots & \varphi_{N,M} \end{pmatrix} \quad (2)$$

The element  $\varphi_{i,j}$  at the right hand side of Eq.2 stands for complex amplitudes of fundamental eigenmode within  $i^{\text{th}}$  single-mode waveguide at right side, which is caused by a unit fundamental eigenmode field incident from  $j^{\text{th}}$  single-mode waveguide at left side.

Similarly, the field at left side  $\Psi_{left}$  could be related to the field at right side  $\Psi_{right}$  by,

$$\Psi_{left} = \mathbf{T}' \Psi_{right} \quad (3)$$

where the prime over  $\mathbf{T}$  stand for transposition and

$$\hat{\mathbf{T}} = \begin{pmatrix} \varphi_{1,1} & \cdots & \varphi_{N,1} \\ \vdots & \ddots & \vdots \\ \varphi_{1,M} & \cdots & \varphi_{N,M} \end{pmatrix}$$

If we transform the field  $\Psi_{right}$  at right side to its conjugation with the help of phase modulation section PS and reflection of DBG as illustrated in Fig.1, using Eq.3, the reflected light field at left side would be,

$$\Psi_{left}^{re} = \mathbf{T}' \overline{\Psi_{right}} \quad (4)$$

Substitute Eq.1 into Eq.4, we get,

$$\Psi_{left}^{re} = \mathbf{T}' \overline{\mathbf{T} \Psi_{left}} \quad (5)$$

Suppose a fundamental eigenmode light field with unit intensity incidents from  $j^{\text{th}}$  single-mode waveguide at left side of the Fig.4. We have  $\Psi_{left-j} = [a_1=0, a_2=0, \dots, a_j=1, \dots, a_M=0]^T$ . From Eq.5 and the fact that  $\mathbf{T}' = \mathbf{T}^T$ , we have

$$a_j^{re} = \bar{a}_j \cdot \sum_{s=1}^M \varphi_{s,j} \overline{\varphi_{s,j}} \quad (6)$$

where  $\varphi_{s,j}$  is element of  $\mathbf{T}$ . Based on the energy conservation theorem and our assumption that reflection is negligible,  $\varphi_{s,j} \overline{\varphi_{s,j}} = 1$ . Applying this to all eigenmodes show that the matrix  $\mathbf{T}' \overline{\mathbf{T}}$  is a unit matrix. In this situation,

$$\Psi_{left}^{re} = \overline{\Psi_{left}} \quad (7)$$

Eq.7 implies that the reflected conjugate light field would return to the same waveguide at left side due to reciprocity and restored the original input light field in its conjugate form.

If radiation modes were generated, a fraction of incident field would radiate away from the core and become inaccessible in later phase conjugate reflection operation. Even if all the radiation modes could be reflected back they would decay exponentially with distance due to their complex propagation constants. In reality, the generation of radiation modes changes the relative strength of guided modes. Therefore in both cases optical phase conjugate reflection becomes imperfect or the optical path is not strictly reciprocal. Definitely, conditions for optical path reciprocity are that there should be no reflection and no radiation modes. Accordingly the waveguide structure AWS in Fig.4 should be adiabatic. That is why we name it as AWS.

### 2.3. Backward digital optical phase conjugation implementation

In this section we show a practical implementation of DOPC. In addition to the conditions for optical reciprocity realization, to carry out DOPC one should know how to measure the decomposed fundamental mode field within the single-mode waveguide and how to create their conjugate light field. We describe the design of components that are essential for DOPC and demonstrate DOPC implementation with FDTD simulations.

#### 2.3.1. Optical multimode interference (MMI)

For the AWS in Fig.1, we can choose in particular an optical  $N \times N$  multimode interferometer (MMI) coupler. MMI couplers are based on the self-imaging effect and are widely used in integrated optics (Soldano L. B. and Pennings E. C. M, 1995). They have many advantages such as compact size, low insertion loss, low polarization dependency, relatively wide bandwidth and good fabrication tolerances.

If a MMI has a width of  $W_0$ , its effective width is (Soldano L. B. and Pennings E. C. M, 1995)

$$W_e = W_0 + \left(\frac{\lambda}{\pi}\right) \left(\frac{n_0}{n_1}\right)^{2\nu} (n_1^2 - n_0^2)^{-0.5} \quad (8)$$

Where  $\nu = 0$  for TE (transverse electric) and  $\nu = 1$  for TM (transverse magnetic) polarization and  $n_1$  and  $n_0$  effective refractive index of the core and cladding respectively.  $\lambda$  is a free-space wavelength of modes supported by the multimode waveguide. The propagation constants for mode  $s$  is

$$\beta_s \cong k_0 n_1 + \frac{(s+1)^2 \pi \lambda}{4 n_1 W_e^2} \quad (9)$$

While the beat length is

$$L_c = \frac{\pi}{\beta_0 - \beta_1} \cong \frac{4 n_1 W_e^2}{3 \lambda} \quad (10)$$

In general,  $N$ -fold images are obtained at distance

$$L = \frac{q}{N} (3L_c) \quad (11)$$

where  $q \geq 0$  and  $N \geq 1$  are integers with no common divisor.

At the distance  $z = L$ ,  $N$  images are formed of the extended input field located at the positions  $x_k$  each

with amplitude  $\frac{1}{\sqrt{N}}$  and phase  $\varphi_{j,k}$  like in Eq.12 for  $q = 1$ .

$$\varphi_{j,k} = \begin{cases} \frac{\pi}{4N}(k-j)(2N+j-k) + \pi & \text{if } j+k = \text{even} \\ \frac{\pi}{4N}(k+j-1)(2N-j-k-1) & \text{if } j+k = \text{odd} \end{cases} \quad (12)$$

where  $j=1,2,\dots,N$  is the index of waveguides on the left side counted bottom-up,  $k=1,2,\dots,N$  is the index of waveguides at right side counted top-down. MMI fulfills then the requirements for the knowledge of measure of the decomposed field. Eq.12 tells then the amplitude and phase of the decomposed eigenmode fields in each single mode waveguide at the right side of MMI.

Therefore, an  $N \times N$  MMI is designed if we place  $N$  single-mode waveguides at both sides of a multimode waveguide of length like in Eq11. The  $N$  single-mode waveguides at both sides are separated in  $X$  direction by distance  $d = \frac{W_e}{N}$ . For a properly designed MMI, an input from one waveguide at left side will be divided equally to all the waveguides at the right side. This is very desirable in our application to perform DOPC because if the decomposed fields in each single-mode waveguide at the right side have equal amplitudes, we only need to modulate phase.

Figure 2 illustrates a FDTD simulation of  $4 \times 4$  MMI for a TE polarized light signal of  $\lambda=1.55 \mu\text{m}$ . The Wafer Dimensions are  $500.00 \mu\text{m}$  (length)  $\times$   $20.00 \mu\text{m}$  (width). The refractive indexes are 3.39 and 3.17 for core and cladding respectively. The length and width of the MMI are  $315 \mu\text{m}$  and  $12 \mu\text{m}$  respectively. The single-mode waveguides are  $0.64 \mu\text{m}$  wide. From Fig.5 we can see that the field incident from the uppermost waveguide at the left side is decomposed equally into four single-mode waveguides at the right side. One can also see that there is almost no reflection, indicating that it is a good choice to take MMI as AWS.

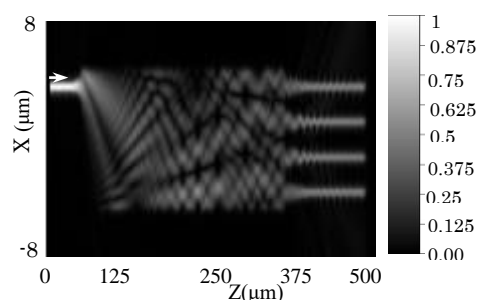


Figure 2.  $4 \times 4$  MMI simulation for  $\lambda = 1.55 \mu\text{m}$

### 2.3.2. Phase modulation mechanism

The phase modulation for conjugation is performed under the control of digitally generated voltage in P elements (Fig.1) where the refraction index of electro-optical material on each waveguide at right side is accurately changed by an amount of  $\Delta n_k$  as in Eq.13.

$$\frac{2\pi}{\lambda_m} \Delta n_k (2L) = \overline{\varphi_{j,k}} - \varphi_{j,k}, \quad k = 1, \dots, N \quad (13)$$

where  $\lambda_m$  is the wavelength in free space,  $L$  the length of each phase shift element and  $\varphi_{j,k}$  phase of the light field from port  $j$  to port  $k$  at the right side of the MMI. The right side of Eq.13 stands for the phase difference between reflected conjugate field and original field. Since the reflected field passes two times through the element P, there is a factor 2 before length  $L$  at the left side of Eq.13.

### 2.3.3. Distributed Bragg grating mirror

DBG is a waveguide with an alternative change of material in the guiding core. This results in periodic variation in the effective refractive index in the guide. As it is illustrated in the Fig.3 (a), each layer boundary causes a partial reflection of the light signal. For signals whose wavelength is close to four times the optical thickness of the layers as in Eq.14, the many reflections combine with constructive interference, and then the layers act as a high-quality reflector. The same function is performed with distributed Bragg reflector (DBR). A DBR has a structure as is illustrated in Fig.3 (b). The core is corrugated in square, rectangular or sinusoidal shape. The depth of the corrugation will determine the effective refractive index contrast in the periodic corrugations. The condition of the Bragg wavelength is the same like for DBG. For maximum reflection,

$$\lambda_B = 4(n_{eff1} * d_1 + n_{eff2} * d_2) \quad (14).$$

The wavelength  $\lambda_B$  in Eq.14 is called Bragg wavelength. For a DBG with enough length  $L$ , the field will be totally reflected and thus the DBG acts as a perfect mirror. DBG can work as band stop filter in addition to mirror. It can have a key role in wavelength selectivity for optical devices.

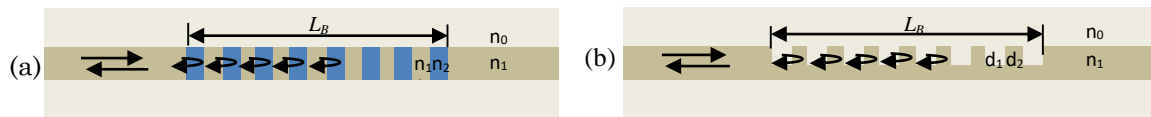


**Figure 3.** DBG (a) and DBR (b) structure.

### 2.3.4. DOPC simulation

In principle, the reflected and modulated light signal in each single-mode waveguide like in Eq.15 will recombine in the MMI and restore the inputted field according to the reciprocity of an optical path.

$$\overline{\psi_{right}} = [\overline{\varphi_{1,j}}, \overline{\varphi_{2,j}}, \dots, \overline{\varphi_{N,j}}]^T \quad (15)$$

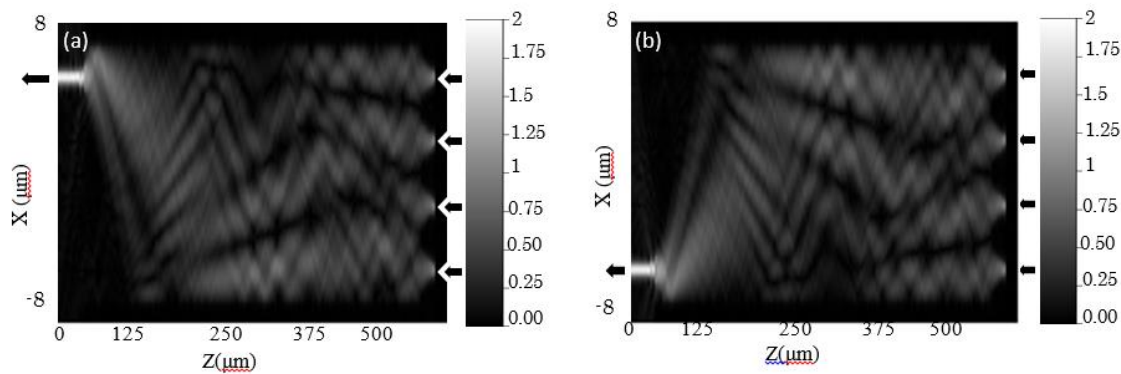


**Figure 4.** FDTD simulation for verification of Eqs.12-13.

Nevertheless, we still need to verify whether the phase calculated with Eq.12 and shifted with Eq.13 is accurate or not for DOPC implementation. Fig.4 is FDTD simulations of how conjugate light signals from single-mode waveguides at right side combine and restored the supposed original input field at left side. The refractive indexes are 3.3737 and 3 for core and cladding respectively. The width of the MMI is 12  $\mu\text{m}$  and the length 310  $\mu\text{m}$ . The wavelength is  $\lambda=1550$  nm. Then for  $j=4$  and  $j=1$ , which means the original light signal is supposed to input at the 4<sup>th</sup> waveguide in Fig. 4(a) and 1<sup>st</sup> waveguide in Fig.4(b) at the left side counted from bottom, the conjugate light signals at right side were given the same amplitude and phase calculated with Eq. 12 and shifted with Eq.13. From the simulation results we can see that the conjugate light signals combined to restore the original input light field at exactly the same  $j^{\text{th}}$  waveguide at the left side as we supposed. Since the light fields in Fig.4 (a)-(b) were in TE and TM modes respectively, the results show that calculated phases with Eq.12 are accurate and can be used for DOPC for both polarizations.

Figure 5 illustrates simulation for DOPC using device like is in the Fig.1. The device is supposed to be constructed on InP substrate (InGaAsP/InP). The refractive index of the core is 3.39 while that for

cladding is 3.17. Each single-mode waveguides is 0.64  $\mu\text{m}$  wide and the length of the MMI is  $L=315.2925$   $\mu\text{m}$ . The light signal was inputted in the 4<sup>th</sup> input port in Fig.5 (a) , 1<sup>st</sup> in Fig.5 (b), 3<sup>rd</sup> in Fig.5 (c) and 2<sup>nd</sup> input port in Fig.5 (d) at a position  $z = 5.6$   $\mu\text{m}$  . It is shown by simulations in those figures that the light field is reconstructed at the very same position inputted. This is done for all polarizations (TE and TM). The fact that DOPC works for all polarizations is advantageous for devices based on the phenomena because when constructed, one will not be obliged to have one for a polarization. A one dimensional field distribution along X direction at the position  $z=1$   $\mu\text{m}$  is plotted at the left side in Fig.5 (a) and (b). The field distribution is for the reflected one because its position is before the source ( $z=1$   $\mu\text{m}$  and for the source  $z=5.6$   $\mu\text{m}$  ). The plot shows that the field reflects at almost 90%. The mirror used to reflect the light is a DBR with  $d_1=d_2=0.1169$   $\mu\text{m}$ . The elements PS has a length of 80 $\mu\text{m}$ . The phase modulation for each element PS was calculated using Eqs.12-13.The simulation shows that the light is reflected back to the same place where it was inputted with slight loss. This is then due to DOPC principle. The loss is generally called insertion loss. It is common that every device has insertion loss. The issue can be if the loss is acceptable or not for a specific application

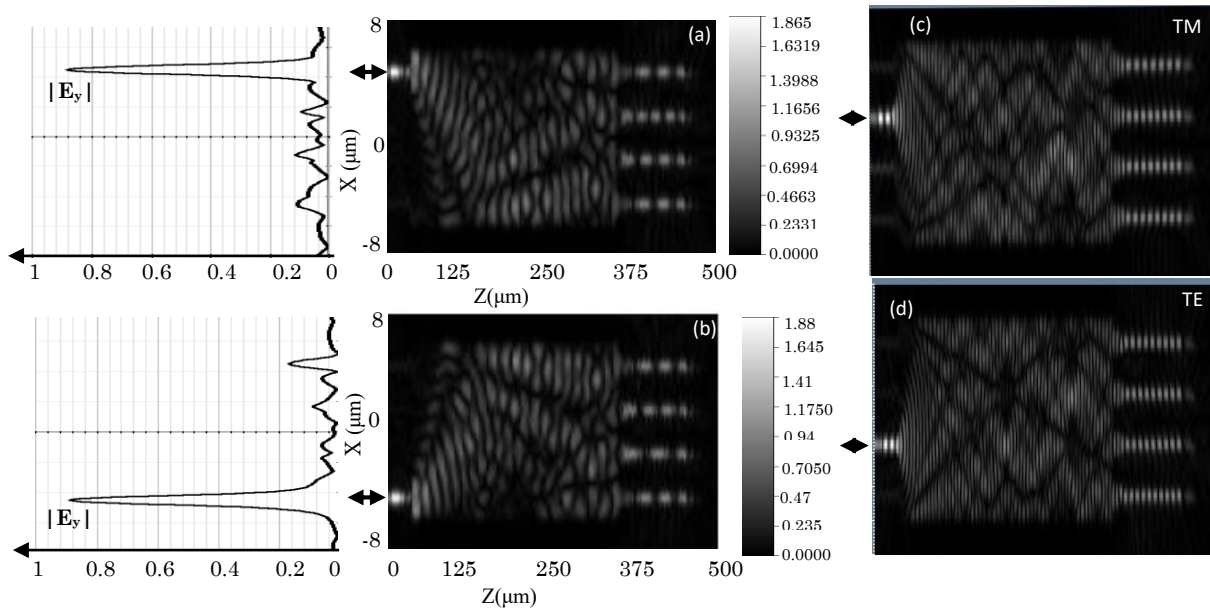


**Figure 5.** DOPC simulation for  $\lambda=1550$  nm TE mode to port 1, 2 and 4 and TM mode for 3.

**3. Forward digital optical phase conjugation**

As stated in the previous section, DOPC allows field reconstruction in the backward direction. In other words, both input and output waveguides are located at the same side of MMI. If we introduce another MMI as illustrated in Fig.6 we can also perform DOPC in forward direction. The design is similar to a  $N \times N$  MMI-MZI structure (Jin Z. et al, 2005; Abdulaziz M A

et al, 2011)). In forward DOPC, DBG for reflection are not needed. We can perform DOPC by phase modulation in PS sections (Fig. 6) like for backward DOPC. The only difference is that the length  $L$  is used in Eq.13 instead of  $2L$  and  $u$  and  $v$  are counted in the same order as indicated in Fig 6.

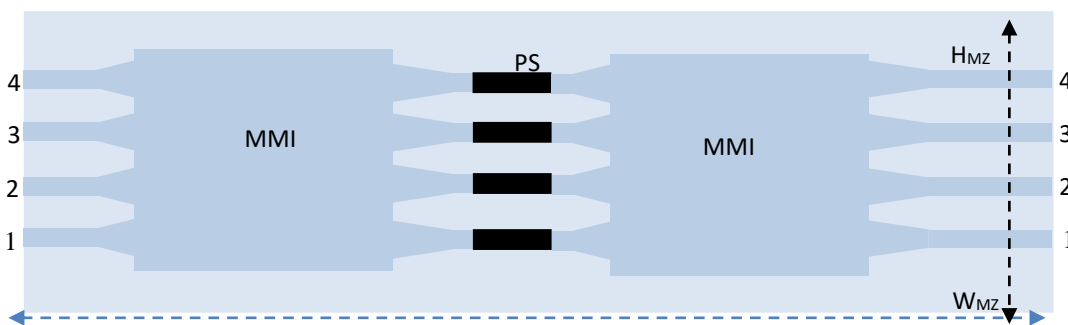


**Figure 6.** Structure for forward DOPC.

Figure 7 illustrates FDTD simulations for forward DOPC for all ports for wavelength 1550 nm. The length of the phase shifter is 80  $\mu\text{m}$ . The in/output port order is counted in the same way: down to top at both left and right sides left and right side of the structure. Inversed order is for the in between waveguides. The arrows indicate light signal propagation direction. The size of the device is  $H_{MZ} \times W_{MZ} = 900 \mu\text{m} \times 16 \mu\text{m}$  for height and wide respectively as illustrated in Fig.6. Light field is reconstructed at the output port at the same position as

the input port (1 to 1, 2 to 2, 3 to 3 and 4 to 4). Forward DOPC from port 1 to 1 is for TM polarized mode. Forward DOPC is also for all polarizations as in backward direction. One dimensional field distribution along X direction at the output ports  $\mu\text{m}$  is plotted at the right side of Fig.7. The one dimensional distribution show the performance a device based on FDOPC should have. One can see from the plot that the field is reconstructed totally at the desired place.

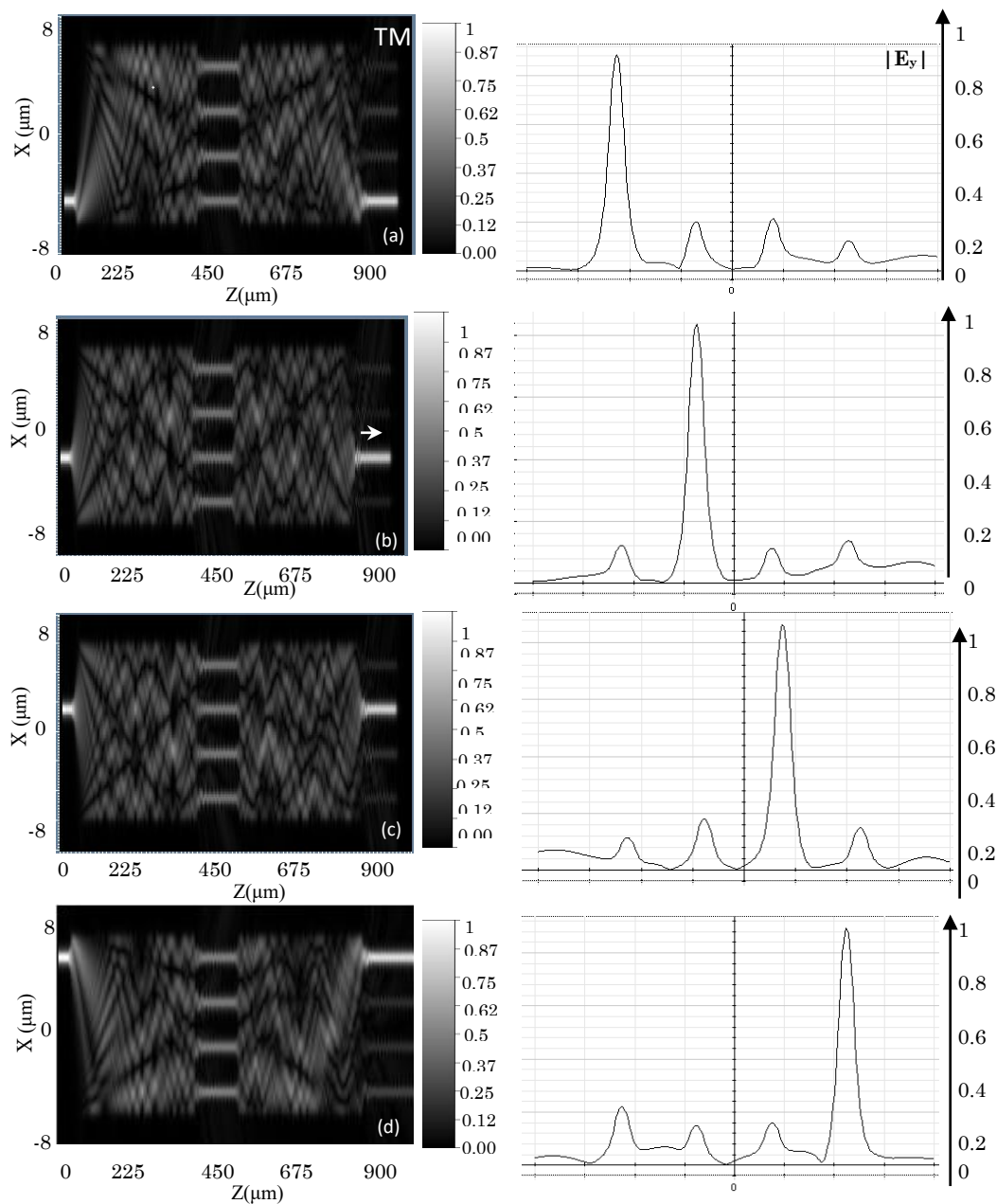


**Figure 7.** Forward DOPC for 1550 nm for all ports and polarization.

#### 4. Conclusion

This paper investigated the possibility to perform DOPC on integrated optical chips both in backward and forward directions. Based on theoretical analyses and numerical simulation by FDTD, It was demonstrated that DOPC can be implemented by first decomposing a complex light field in a waveguide device into a number of single mode waveguides with the aid of a multimode interference coupler. The decomposed fundamental eigenmodes can then be reflected by distributed Bragg grating and digitally modulated via EO effect to their phase conjugation. It was found that DOPC can also be performed in forward direction without need of distributed Bragg grating by only digitally modulate via EO effect modes to their phase conjugation. DOPC is generalized for both directions and all polarizations and allows to reconstruct light field at desired place. Devices designed on DOPC would be of high performance as the one dimensional distribution shows.

#### References

- [1] Yariv A and Yeh P, (1978). Phase conjugate optics and real-time holograph. *IEEE J. Quantum Electron*, 14(9): 650–660.
- [2] Guang S. He. (2002). Optical phase conjugation: principles, techniques and applications. *Progress in Quantum Electronics*, 26: 131–191.
- [3] Feinberg J and Hellwarth R. W. (1980). Phase-conjugating mirror with continuous-wave gain. *Opt. Lett.*, 5(12): 519–521.
- [4] Lindsay. (1987). Specular reflection cancellation enhancement in the presence of a phase-conjugate mirror. *J. Opt.Soc. Am. B*; 4(11):1810–1815.
- [5] Yeh P. (1993). *Introduction to photorefractive nonlinear optics*. John Wiley & Sons, Inc, New York,. ISBN: 978-0-471-58692-0
- [6] Meng C and Changhui Y. (2010). Implementation of a digital optical phase conjugation system and its application to study the robustness of turbidity suppression by phase conjugation. *OPTICS EXPRESS*, Vol. 18, No. 4: 3444.
- [7] Zhiyang Li (2010). Accurate optical wavefront reconstruction based on reciprocity of an optical path using low resolution spatial light modulators. *Optics Communications*, 283:3646–3657.
- [8] Miller S.E. (1969) *Integrated Optics: An Introduction*. *Bell Syst. Tech. J.*, 48:2059-2069.
- [9] Soldano L. B. and Pennings E. C. M. (1995) *Optical Multi-Mode Interference Devices Based on Self-Imaging: Principles and Applications*. *Journal of Lightwave Technol*, 13 (4):615-627.
- [10] Zhiyang L. (2013). 3D display based on complete digital optical phase conjugation. *Optics Communications*, 293: 10–14.
- [11] Songcan L and Mark N A. (2000). Digital wavefront reconstruction and its application to image encryption. *Optics Communications.*, 178: 283–289
- [12] Hsieh C.L, Pu Y, Grange R and Psaltis D. (2010). Digital phase conjugation of second harmonic radiation emitted by nanoparticles in turbid media. *OPTICS EXPRESS*, Vol. 18, No. 12: 12283.
- [13] Gower D. P. M. (1994). *Optical phase conjugation*. Springer-Verlag, New York.
- [14] Jansen S L (2006). *Optical phase conjugation in fiber-optic transmission systems*. Ph.D thesis, Netherlands .Technishe Univeriteit Eindhoven.
- [15] Zhiyang L and Havyarimana C. (2013). Compact wavelength-selective optical switch based on digital optical phase conjugation. *Opt. Lett.*, 38: 4789-4792.
- [16] Havyarimana C and Zhiyang L, (2015), Architecture to Integrate a Large-Scale DOPC-Based Optical Switching System on a Chip, *J. Opt. Commun. Netw./Vol. 7, NO. 7*
- [17] Yuecheng S, Yan L, Cheng M and Lihong V. W. (2016). Focusing light through scattering media by full-polarization digital optical phase conjugation. *Opt. Lett*, 41: 1130-1133.
- [18] Jin Z, Kaalund C J and Peng G. (2005). Novel Approach to Design High-Performance Large-Port-Count Switches in Low-Index- Contrast Materials Based on Cascaded Multimode Interference Couplers. *IEEE journal of quantum electronics*, 41:1548-1551.
- [19] Abdulaziz M A H, Abu Bakar M, Abu Sahmah M. S and Zaid A S. (2011). MMI-MZI Polymer Thermo-Optic Switch with a High Refractive Index Contrast. *J. Lightwave Technol.*; 29: 171-178.
- [20] Yu,Z., Xia, M., Li, H. *et al.* (2019) Implementation of digital optical phase conjugation with embedded calibration and phase rectification. *Sci Rep* 9, 1537. <https://doi.org/10.1038/s41598-018-38326-4>
- [21] Kai Zhang 1, Zhiyang Wang 2,y, Haihan Zhao 3, Chao Liu 3, Haoyun Zhang 3 and Bin Xue 3,\* (2020), Implementation of an Off-Axis Digital Optical Phase Conjugation System for Turbidity Suppression on Scattering Medium *Appl. Sci.*, 10, 875; doi:10.3390/app10030875

- [22] Zhongtao Cheng, Jiamiao Yang, and Lihong V. Wang, (2020) "Intelligently optimized digital optical phase conjugation with particle swarm optimization," *Opt. Lett.* 45, 431-434
- [23] Chaojie Ma, Jianglei Di, Yi Zhang, Peng Li, Fajun Xiao, Kaihui Liu, Xuedong Bai, and Jianlin Zhao, (2018) "Reconstruction of structured laser beams through a multimode fiber based on digital optical phase conjugation," *Opt. Lett.* 43, 3333-3336
- [24] Ivo M. Vellekoop, Meng Cui, and Changhui Yang (2012); Digital optical phase conjugation, *Appl. Phys. Lett.* 101, 081108 <https://doi.org/10.1063/1.4745775>
- [25] Hillman, T., Yamauchi, T., Choi, W. *et al.* (2013), Digital optical phase conjugation for delivering two-dimensional images through turbid media. *Sci Rep* 3, 1909. <https://doi.org/10.1038/srep01909>
- [26] Daifa Wang, Edward Haojiang Zhou, Joshua Brake, Haowen Ruan, Mooseok Jang, and Changhui Yang, (2015) "Focusing through dynamic tissue with millisecond digital optical phase conjugation," *Optica* 2, 728-735
- [27] Chaojie Ma, Jianglei Di, Yi Zhang, Peng Li, Fajun Xiao, Kaihui Liu, Xuedong Bai, and Jianlin Zhao, (2018) Reconstruction of structured laser beams through a multimode fiber based on digital optical phase conjugation, *Optics Letters*, Vol. 43, Issue 14, pp.3333-3336 <https://doi.org/10.1364/OL.43.003333>